Delimiting Subterritories of the Human Subthalamic Nucleus by Means of Microelectrode Recordings and a Hidden Markov Model

Adam Zaidel, MSc,[1,2]* Alexander Spivak, MD,[3] Lavi Shpigelman, PhD,[1,2]
Hagai Bergman, MD, PhD,[1,2,4] and Zvi Israel, MD[3]

[1]*Interdisciplinary Center for Neural Computation, The Hebrew University, Jerusalem, Israel*
[2]*Department of Physiology, The Hebrew University–Hadassah Medical School, Jerusalem, Israel*
[3]*Department of Neurosurgery, Hadassah University Hospital, Jerusalem, Israel*
[4]*Eric Roland Center for Neurodegenerative Diseases, The Hebrew University, Hadassah Medical School, Jerusalem, Israel*

Abstract: Positive therapeutic response without adverse side effects to subthalamic nucleus deep brain stimulation (STN DBS) for Parkinson's disease (PD) depends to a large extent on electrode location within the STN. The sensorimotor region of the STN (seemingly the preferred location for STN DBS) lies dorsolaterally, in a region also marked by distinct beta (13–30 Hz) oscillations in the parkinsonian state. In this study, we present a real-time method to accurately demarcate subterritories of the STN during surgery, based on microelectrode recordings (MERs) and a Hidden Markov Model (HMM). Fifty-six MER trajectories were used, obtained from 21 PD patients who underwent bilateral STN DBS implantation surgery. Root mean square (RMS) and power spectral density (PSD) of the MERs were used to train and test an HMM in identifying the dorsolateral oscillatory region (DLOR) and nonoscillatory subterritories within the STN. The HMM demarcations were compared to the decisions of a human expert. The HMM identified STN-entry, the ventral boundary of the DLOR, and STN-exit with an error of -0.09 ± 0.35, -0.27 ± 0.58, and -0.20 ± 0.33 mm, respectively (mean $\pm$ standard deviation), and with detection reliability (error < 1 mm) of 95, 86, and 91%, respectively. The HMM was successful despite a very coarse clustering method and was robust to parameter variation. Thus, using an HMM in conjunction with RMS and PSD measures of intraoperative MER can provide improved refinement of STN entry and exit in comparison with previously reported automatic methods, and introduces a novel (intra-STN) detection of a distinct DLOR-ventral boundary. © 2009 Movement Disorder Society

Key words: deep brain stimulation; Parkinson's disease; functional neurosurgery; beta oscillations

Surgical treatment for advanced Parkinson's disease (PD) includes deep brain stimulation (DBS) of the subthalamic nucleus (STN), which has proven to be safe and beneficial over time.[1–3] During surgery for implanting an STN DBS macroelectrode, microelectrode recording (MER) is often utilized to verify localization of the STN physiologically.[4–6] To implant the macroelectrode successfully within the optimal location (probably the sensorimotor portion of the STN),[7] accurate demarcation of the patient's STN (based on the MERs) is required. This includes derivation of the entry and exit points of the STN across the MER trajectory, as well as localization of the sensorimotor area within the STN.

It has been well established that the STN can be divided into three (sensorimotor, limbic, and cognitive/associative) functional territories, each broadly involved in its respective basal ganglia–thalamocortical loop.[8–13] The sensorimotor region of the STN is primarily located dorsolaterally,[14–17] the same location that seems to provide optimal therapeutic benefit to patients undergoing STN DBS.[18–21]

Furthermore, it has been shown that local field potential[22–24] and single unit[25] (when averaged across patients) beta oscillatory activity is generated largely

within the dorsolateral portion of the STN. It would therefore seem that there is correspondence between the dorsolateral oscillatory region (DLOR) and the sensorimotor region of the STN, and that beta-oscillatory activity could possibly predict the most effective contact for STN DBS.[26,27] The extent of this overlap (DLOR, sensorimotor STN region, and optimal DBS location), however, still requires further investigation. This manuscript is limited to the development of a reliable, real-time method that can be applied to a single STN MER penetration.

Such a method could aid the neurosurgeon in implanting the macroelectrode in the optimal location or simply be used to estimate the transitions of a MER trajectory. Automatic methods have been described to identify the entry and exit points of the STN;[28–30] however, to the best of our knowledge there is no physiological method described to date that identifies subterritories within the STN. We present in this article a real-time method to delimit the outer boundaries of the STN as well as an intra-STN (DLOR-ventral) boundary during surgery based on the root mean square (RMS) and power spectral density (PSD) of the MERs, using a Hidden Markov Model (HMM).[31]

PATIENTS AND METHODS

Patients and MERs

The MERs from 21 PD patients undergoing bilateral STN DBS implantation were analyzed (patient details are presented in Table 1). All patients met accepted selection criteria for STN DBS and signed informed consent for surgery with MER. This study was authorized and approved by the Institutional Review Board of Hadassah University Hospital in accordance with the Declaration of Helsinki. No sedative was used and all patients were awake during surgery. The patient's level of awareness was continuously assessed clinically, and when drowsy the patient was stimulated and awoken through conversation by a member of the surgical team. Data were obtained off dopaminergic medications (>12 hours since last medication) and during periods of rest. Further details of the surgical procedure and data acquisition are presented as supplementary material.

For both the left and right hemispheres, a single trajectory using one or two microelectrodes (separated by 2 mm anteroposteriorly in the parasagittal plane) was made starting at 10 mm above the calculated target (center of the lateral STN). The electrodes were advanced in small discrete steps, toward the estimated

center of the lateral STN. Step size (ranging 500 μm down to 50 μm in our recordings) was controlled by the neurophysiologist in order to achieve optimal unit recording and identification of upper and lower borders of the STN. Typically, shorter steps (~100 μm) were used when the electrode was advanced closer to the presumed location of the STN. Following a 2-second signal stabilization period after electrode movement cessation, multi-unit traces were recorded for a minimum of 5 seconds. All stable sections included in the analysis (after automatic stability analysis – see supplementary information) were longer than 3 seconds (duration mean ± SD: 10.8 ± 3.4 seconds). Only electrodes that passed through the STN were used for this study (56 in total).

The RMS and PSD

Entry and exit from the STN are marked primarily by a dramatic increase and decrease in normalized RMS (NRMS), respectively.[29,32,33] In addition, PSD can be used as a marker for the DLOR of the STN based on the increased beta oscillatory activity. The NRMS and PSD of an example trajectory, as a function of estimated distance to target (EDT), are presented in Figure 1. When plotting the PSD, the 50 Hz power supply artifacts and their harmonics were replaced by the mean PSD, and the PSD was smoothed in the frequency direction using a narrow Gaussian window (SD = 0.33 Hz). The methods used for calculating the NRMS and PSD are presented in the supplementary material.

The Hidden Markov Model

A HMM was used to estimate the state of the electrode at each depth across the trajectory based on the NRMS and PSD of the MERs. Four discrete states were defined:

1. Before the STN
2. In the DLOR of the STN
3. In the nonoscillatory STN
4. Out of the STN

A typical trajectory state sequence would go through all four states consecutively. However, not all trajectories had oscillatory recordings in the presumed dorsolateral region of the STN; hence, a trajectory could skip state 2. In addition, it was possible for a trajectory to end in state 3 (a MER trajectory that was terminated before exiting the STN). In the advancement of a sequence, it was possible to remain in the same state,

TABLE 1. *Patient details*

	Age (yr)	Gender	Disease duration (yr)	UPDRS before DBS		UPDRS after DBS					Medications (LEDD*) daily doses		
				On Med	Off Med	Months since DBS	On Stim		Off Stim		Before STN DBS	Months since DBS	After STN DBS
							On Med	Off Med	On Med	Off Med			
Patient 1	73	F	14	31	70	NA	NA	NA	NA	NA	2250	3	950
Patient 2	51	F	14	17	99	13	2	16	9	46	1700	NA	875
Patient 3	68	M	9	NA	NA	NA	NA	NA	NA	NA	1662.5	NA	1246.9
Patient 4	69	M	10	32	65.5	NA	NA	NA	NA	NA	375	NA	412.5
Patient 5	61	F	11	NA	NA	10	11	NA	NA	54	1087	9	0
Patient 6	58	M	22	22.5	55	8	5	14	61	64	2575	8	900
Patient 7	57	M	10	NA	NA	8	0	14	NA	65	1250	8	250
Patient 8	73	M	6	22	55	4	5	18	NA	NA	1700	NA	700
Patient 9	50	M	8	29	79	2	14	12	47	54	379.5	NA	259.5
Patient 10	75	F	8	17	51	8	17	21	24	37	1400.1	7	897.8
Patient 11	61	M	6	20	47	8	10	25	NA	NA	399	6	266
Patient 12	61	F	5	38	73	8	1	10	NA	47	1250	5	125
Patient 13	56	M	8	29	70	NA	NA	NA	NA	NA	875	NA	250
Patient 14	63	F	12	19	49	3	5	16	NA	NA	890	NA	459
Patient 15	49	M	10	4	44	NA	NA	NA	NA	NA	900	NA	NA
Patient 16	64	F	11	3	21	5	2	4	7	21	1505	4	437.5
Patient 17	52	M	9	13	49.5	1	6	22	NA	34	1300	3	312.5
Patient 18	59	M	8	13	72	1	9	30	NA	49	725	NA	248.7
Patient 19	61	M	6	32	60	3	10	14	51	61	700	2	200
Patient 20	55	M	7	21	37	3	8	15	17	21	740	NA	426
Patient 21	66	F	15	NA	NA	NA	NA	NA	NA	NA	1540	3	375
Mean	61.0	38% F	10.0	21.3	58.6	5.7	7.0	16.5	30.9	46.1	1200.1	5.3	479.6

*LEDD, levodopa equivalent daily dose as calculated by Deuschl et al.[34]
DBS, deep brain stimulation; Med, medication; Stim, stimulation; UPDRS, Unified Parkinson's Disease Rating Scale – motor section (section 3, maximum = 108); NA, not available.
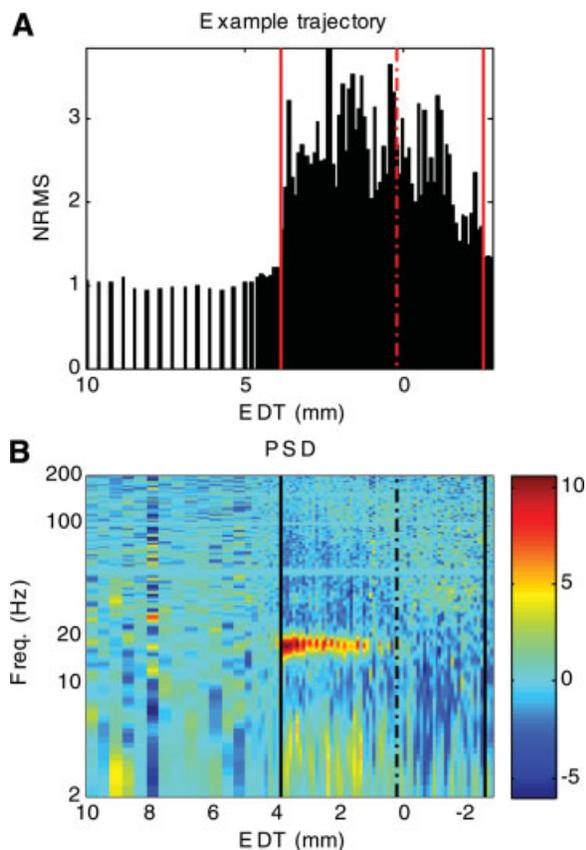
FIG. 1. (**A**) The NRMS of an example trajectory (Patient 17, right STN) as a function of estimated distance to target (EDT). (**B**) The PSD of the same trajectory. The PSD color-scale represents $10 \times \log_{10}$ (PSD power/average PSD power) per EDT. The red (A) and black (B) solid vertical lines indicate STN entry and exit; the dot-dash lines indicate the ventral boundary of the dorsolateral oscillatory region (DLOR).

but not possible to go backwards (e.g., from a state within the STN to "before the STN" state). Trajectories that did not pass through the STN were not included in this study because they are a trivial case for which the RMS remains at baseline level throughout the trajectory and there are no transitions. (For an online application, it could be easily tested whether the RMS has a minimum increase before applying the HMM to the trajectory.)

An HMM state sequence uniquely defined three possible state transitions:

  i. In: STN entry (noted by transition from state 1 to state 2 or state 3).
  ii. DLOR-ventral: the ventral boundary of the DLOR (noted by transition from state 2 to state 3).
  iii. Out: STN exit (noted by transition from state 3 to state 4).

A scheme of the possible HMM states and transitions can be seen in Figure 2.

Data Observations and Clustering

In order to best estimate the hidden state, the following observations were used:

  1. The normalized root mean square (NRMS)
  2. The mean beta (13–30 Hz) PSD
  3. The maximum beta PSD

Since the data set was limited (56 trajectories), it was necessary to have a relatively small HMM "emission" matrix (the matrix depicting the probability of each observation per HMM state) otherwise it wouldn't be adequately sampled during the learning stage. This requirement limited the resolution with which the three different observation quantities could be quantized since the number of possible combinations defines the order of the matrix. A custom method of coarse (yet logical, as will be explained below) quantization was adopted, whereby the observations were grouped into six clusters as follows:

  • All observations with NRMS < 1.25 (threshold 1), i.e. below a 25% increase from the NRMS baseline (which is equal to 1 due to the normalization) were clustered together (Low-NRMS cluster).
  • The mean deviation from threshold 1 (i.e. NRMS − 1.25) of the remaining observations was calculated. Threshold 2 was defined by threshold 1 plus 25% of the calculated mean deviation. Observations with NRMS between threshold 1 and threshold 2 were clustered together (Intermediate-NRMS cluster), while observations with NRMS > threshold 2 where further divided according to their (maximum and mean) beta oscillatory activity (above or below the median), resulting in a further four (high-NRMS) clusters (a detailed breakdown of these clusters can be seen in the Supporting Information Table S1B).

The reasoning behind the clustering method can be explained as follows: In clustering the NRMS, using
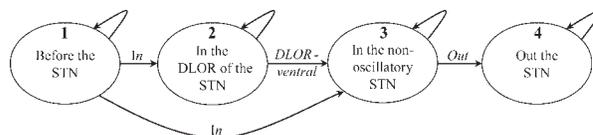

FIG. 2. The four possible HMM states. Arrows represent the three possible states transitions (In, DLOR-ventral, and Out) and the possibility of staying in the same state with no transition (reflexive arrows).
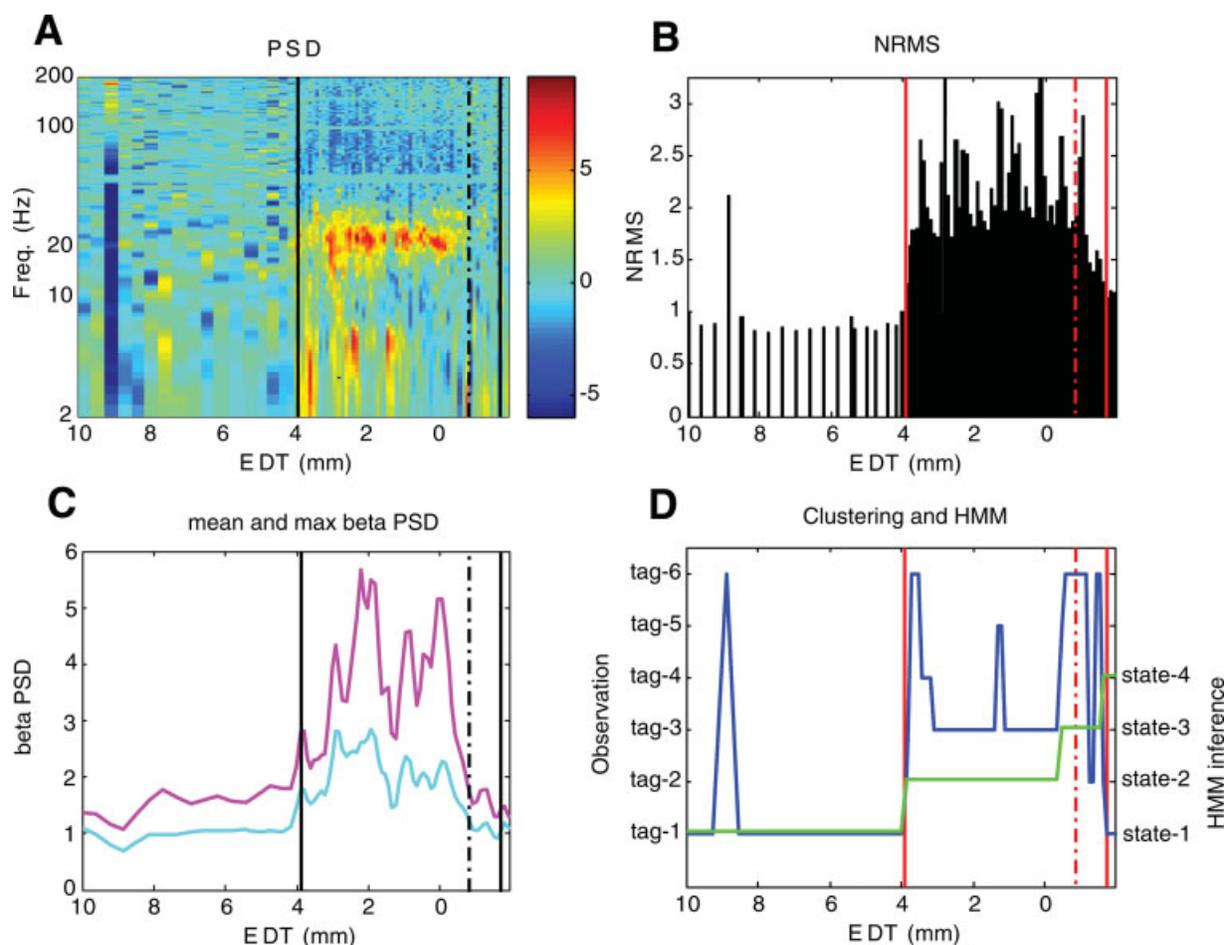
FIG. 3. An HMM transition inference example (Patient 13, right STN). (**A**) PSD, same conventions as in Figure 1B. (**B**) NRMS, same conventions as in Figure 1A. (**C**) Cyan and magenta lines represent the mean and maximum beta PSD, respectively. Beta PSD per EDT $=10 \times \log_{10}$ (PSD power/average PSD power). (**D**) The blue and green lines represent the cluster observation sequence (tags) and the HMM state inference (states, as defined in Fig. 2), respectively.

an "absolute" threshold (threshold 1) was appropriate since the RMS was normalized. However, as we have previously reported,[32] there exists interpatient variability of NRMS within the STN; hence, it is also appropriate to have a "relative" threshold in addition (threshold 2) particular to each trajectory. The NRMS values (and less so PSD) are important in deciding In/Out transitions; hence, PSD was not taken into account for low NRMS values. However, for high NRMS (>threshold 2), the observations were further clustered based on the PSD since the DLOR-ventral transition (based on PSD) takes place at high values of NRMS (i.e. within the STN). It was noted that some patients had a narrow band of beta oscillatory activity (e.g. Fig. 1B), whereas others had a wider band (e.g. Fig. 3A and Supporting Information Fig. S1B,D). We assumed that maximum and mean beta PSD would better capture the narrow

and wide band beta oscillations, respectively. Both mean and maximum (beta oscillatory activity) were used for PSD clustering. Tremor frequency oscillations seemed to be episodic[25] and sporadic. They were not always present and when present they did not define a continuous region as the beta oscillations did (Fig. 3A). We therefore did not incorporate them into the HMM.

Estimating and Testing the HMM

For each trajectory, the "known" state transitions were defined (corresponding to the three possible HMM state transitions—mentioned earlier in section The Hidden Markov model). In (STN entry) and Out (STN exit) transitions were based on intraoperative neuronal analysis by the neurophysiologist as well as the NRMS plots, and the DLOR-ventral transition was

distinguished by visual inspection of the PSD by one of the authors (AZ)—noting a sudden decrease in beta oscillatory activity. The known state transitions are depicted in the NRMS plots by red lines and in the PSD plots by black lines (Figs. 1 and 3). These transitions defined a known state sequence for estimating and testing the HMM.

The maximum likelihood estimate of the HMM transition and emission probability matrices were estimated based on the known (human expert defined) state sequences. Since the training data were fully labeled (there were known state sequences for the whole dataset), there was no need for the expectation-maximization (EM) algorithm or iterative procedures (which would require initial guessing of the probability matrices), and the matrices could be directly estimated. The HMM was estimated using the known state sequences of all trajectories excluding one (N − 1 = 55), and then tested on the excluded trajectory (with no assumption of its sequence) by comparing the inferred HMM state transitions to the trajectory's known state transitions. The inferred HMM state sequence was calculated as the most probable sequence beginning with the HMM in state 1 before the first observation (using the Viterbi algorithm).[31] This method was repeated N (56) times, testing each trajectory individually. The mean and SD of the error in estimating each of the three transitions were calculated.

Software

Data analysis was carried out on custom software, MATLAB V7.1 (Mathworks, Natick, MA), using MATLAB HMM toolbox. The software used in this article can be found online (http://basalganglia.huji. ac.il/links.htm).

RESULTS

Distinct DLOR

The description of beta oscillations in the STN to date has generally been derived from pooling data across patients.[22–25] The pooled data presents a gradient of beta oscillatory activity (more oscillations dorsally; less ventrally) giving the impression of a continuum, without a distinct dorsal-ventral border. Such a mean gradient however does not necessitate that each patient/trajectory has a gradient. Rather it can arise from the pooling of numerous trajectories, each of which has a distinct oscillatory/nonoscillatory boundary but at different depths. The individual trajectories we analyzed demonstrated the existence of a distinct

DLOR boundary and not a gradient (Figs. 1B and 3A). Some trajectories had a short DLOR and others had a longer DLOR (sometimes extending far ventrally) and when pooled the heterogeneous trajectories average to a gradient of beta oscillatory activity. We therefore propose that each trajectory has a distinct boundary (at a particular depth) that can be visually discerned and automatically detected by an HMM.

HMM State Inference

For each of the 56 trajectories, the HMM was estimated individually based on the other 55 trajectories. The resulting mean HMM transition and emission matrices are presented as Supporting Information Table S1. The HMM state sequence of the trajectory being tested was then inferred using the Viterbi algorithm, based on the trajectory's (clustered) NRMS and PSD sequence. Figure 3 shows a typical trajectory's PSD (Fig. 3A) and NRMS (Fig. 3B) as well as the mean and maximum beta oscillatory activity used for clustering (Fig. 3C). Figure 3D presents the tags resulting from clustering (blue line) together with the HMM inferred state sequence (green line). The inferred state transitions are noted by the steps in the state sequence (e.g. a step from state 1 to state 2 signifies the In transition etc.). In this example, the HMM transition inference concurs with the known (expert decision) In and Out transitions (solid red lines), but slightly precedes the known DLOR-ventral transition (dot-dash red line).

For each transition (In, Out, and DLOR-ventral) the state transition error was defined as follows (Eq. 1):

$$\text{Error} = S - \hat{S} \qquad (1)$$

where S is the known state transition defined by the neurophysiologist and $\hat{S}$ is the HMM inferred state transition (Fig. 3, red lines and steps in the green line, respectively) in mm EDT. Hits and Correct Rejections (CRs) were the number of correctly detected and correctly negated transitions respectively. Hits did not take into account detection accuracy, it was simply used to count the number of inferred HMM transitions where there was also a known transition. All Hits, however, were within 2 mm, and 88% of Hits were within 0.5 mm of the known transitions (Fig. 4). Misses were the number of transitions (according to the expert decision) that the HMM did not detect and False Alarms (FAs) were the number of HMM transition detections when by expert decision there was no transition. A histogram of the spatial errors in inferring the location of the state transitions can be seen in
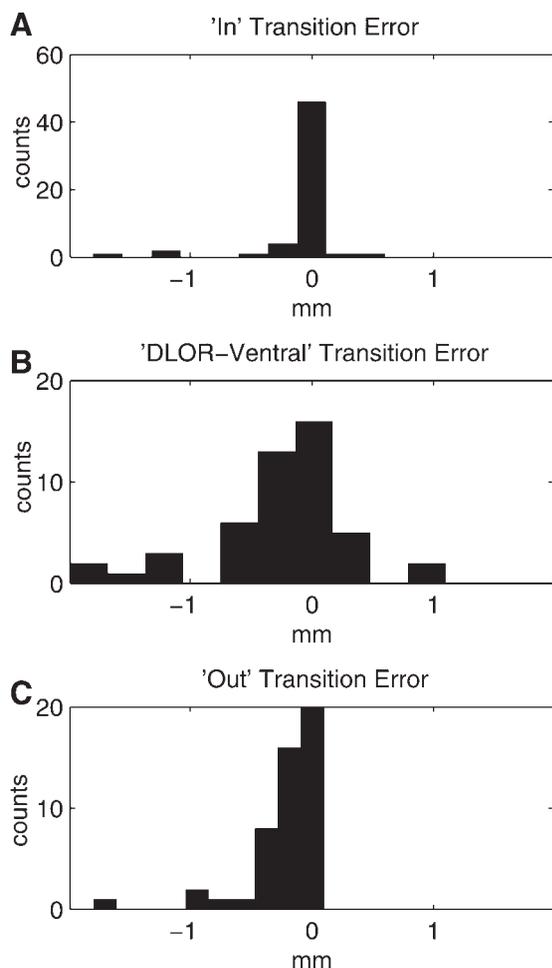
FIG. 4. The HMM transition error histograms for (**A**) In, (**B**) DLOR-ventral, and (**C**) Out state transitions.

Figure 4 and a summary of the results (including Hits, CRs, FAs, and Misses) can be seen in Table 2. Detection reliability (Table 2) was calculated by the sum of correct detections (Hits + CRs) divided by the total number of trajectories. A stricter calculation of detection reliability (limiting Hits to those with error < 1 mm) is also presented in Table 2.

The In transition error described here (mean ± SD: −0.09 ± 0.35 mm) was better than that found by the Bayesian method[29] both in mean and SD (Bayesian method, error = 0.18 ± 0.84 mm). The Out transition error (mean ± SD: −0.20 ± 0.33 mm) also demonstrated better mean and standard deviation (Bayesian method, error = 0.50 ± 0.59 mm). The DLOR-ventral transition detection is novel and therefore doesn't have a reference for comparison, but showed similar results to the In/Out detections (mean ± SD: −0.27 ± 0.58 mm).

The HMM algorithm had to deal with a heterogeneous variation of trajectories (examples are presented in the Supporting Information Fig. S1). While achieving good results despite this challenge (Table 2 and Fig. 4), it failed on occasion. A detailed analysis of the HMM detection errors is presented in the supplementary material. Nevertheless, the HMM proved to be robust. This was tested both by varying the detection thresholds (up and down) and also by removing the stability analysis. Minimal or no effect of these variations was seen on detection accuracy and reliability, demonstrating robustness of the model. A detailed description of the robustness analysis is also presented in the supplementary material.

DISCUSSION

The beneficial effects of bilateral STN DBS on motor symptoms and quality of life have been demonstrated in patients with advanced PD[34]; however, adverse effects of cognitive deterioration or psychiatric complications have also been reported.[35,36] Since the STN has separate sensorimotor, limbic, and cognitive/associative subterritories,[8–17] it would seem probable that accurate implantation of the DBS macroelectrode within the sensorimotor region is essential for achieving therapeutic motor benefit while avoiding limbic or cognitive side effects. Hence, demarcation of the outer boundaries of the STN is not enough, and demarcation

TABLE 2. *A summary of the HMM transition detections, detection reliability, and transition error results*

Transition	Correct detections		Incorrect detections		Reliability = (correct detections / total)		Mean error (mm)	SD of error (mm)
	Hits	CR	Misses	FA	All Hits	Error < 1 mm		
In	56	0	0	0	100%	95%	−0.09	0.35
DLOR-ventral	48	7	0	1	98%	86%	−0.27	0.58
Out	49	3	4	0	93%	91%	−0.20	0.33

The results presented are for all Hits (all Hits were within 2mm of their known transitions, i.e., error < 2 mm). Reliability is presented for all Hits as well as when limiting Hits to error < 1 mm.
CR, correct rejections; FA, false alarms; SD, standard deviation.

of the subterritories of the STN is required. Automatic methods presented to date use MER to localize only the outer boundaries of the STN.[28–30,33] By adding beta PSD analysis and using an HMM, demarcation of subterritories within the STN is possible.

In this study, a very simple (and coarse) clustering technique provided good state inference of the MER trajectory by means of an HMM. Better accuracy than the Bayesian method for detecting STN entry/exit was achieved, with the addition of an intra-STN DLOR-ventral transition detection. The HMM can be used off-line to automatically detect the trajectory state transitions, or semi-online at the end of a trajectory during STN DBS surgery to help refine demarcation of the sensorimotor STN for macroelectrode implantation. Localization of the DLOR-ventral transition can aid the neurosurgeon in deciding which MER track to implant, when multiple electrodes are used for MER, and in implanting the macroelectrode at the optimal depth.

Positive therapeutic benefit to STN-DBS has been associated with proximity of the active macroelectrode contacts to the dorsolateral border of the STN.[18,19,21] It has been proposed that this may be due to activation of adjacent structures such as the zona incerta and/or fields of Forel. We would like to suggest that the benefits of STN dorsolateral border placement of the macroelectrode may also be due to avoidance of volume conduction to ventral areas, which have been associated with neuropsychological side effects.[37,38] If this is the case then electrode distance from the DLOR-ventral border may be of primary importance in achieving optimal sensorimotor benefit without cognitive or limbic side effects.

The good results and robustness of the HMM in this study despite coarse clustering, indicate that higher resolution (calculated across a larger data set) in conjunction with a more advanced HMM—utilizing spike shape and discharge pattern—would probably provide even better results. This should be explored by future studies.

REFERENCES

1. Limousin P, Pollak P, Benazzouz A, et al. Bilateral subthalamic nucleus stimulation for severe Parkinson's disease. Mov Disord 1995;10:672–674.
2. Krack P, Batir A, Van Blercom N, et al. Five-year follow-up of bilateral stimulation of the subthalamic nucleus in advanced Parkinson's disease. N Engl J Med 2003;349:1925–1934.
3. Machado A, Rezai AR, Kopell BH, Gross RE, Sharan AD, Benabid AL. Deep brain stimulation for Parkinson's disease: surgical technique and perioperative management. Mov Disord 2006;21:S247–S258.
4. Sterio D, Zonenshayn M, Mogilner AY, et al. Neurophysiological refinement of subthalamic nucleus targeting. Neurosurgery 2002;50:58–67.
5. Israel Z, Burchiel K. Microelectrode recording in movement disorder surgery. Stuttgart: Thieme; 2004.
6. Gross RE, Krack P, Rodriguez-Oroz MC, Rezai AR, Benabid AL. Electrophysiological mapping for the implantation of deep brain stimulators for Parkinson's disease and tremor. Mov Disord 2006;21(Suppl 14):S259–S283.
7. Starr PA. Placement of deep brain stimulators into the subthalamic nucleus or Globus pallidus internus: technical approach. Stereotact Funct Neurosurg 2002;79:118–145.
8. Alexander GE, Crutcher MD, DeLong MR. Basal ganglia-thalamocortical circuits: parallel substrates for motor, oculomotor, "prefrontal" and "limbic" functions. Prog Brain Res 1990;85:119–146.
9. Parent A, Hazrati LN. Functional anatomy of the basal ganglia. II. The place of subthalamic nucleus and external pallidum in basal ganglia circuitry. Brain Res Brain Res Rev 1995;20:128–154.
10. Shink E, Bevan MD, Bolam JP, Smith Y. The subthalamic nucleus and the external pallidum: two tightly interconnected structures that control the output of the basal ganglia in the monkey. Neuroscience 1996;73:335–357.
11. Joel D, Weiner I. The connections of the primate subthalamic nucleus: indirect pathways and the open-interconnected scheme of basal ganglia- thalamocortical circuitry. Brain Res Brain Res Rev 1997;23:62–78.
12. Hamani C, Saint-Cyr JA, Fraser J, Kaplitt M, Lozano AM. The subthalamic nucleus in the context of movement disorders. Brain 2004;127(Part 1):4–20.
13. Baup N, Grabli D, Karachi C, et al. High-frequency stimulation of the anterior subthalamic nucleus reduces stereotyped behaviors in primates. J Neurosci 2008;28:8785–8788.
14. Monakow KH, Akert K, Kunzle H. Projections of the precentral motor cortex and other cortical areas of the frontal lobe to the subthalamic nucleus in the monkey. Exp Brain Res 1978;33:395–403.
15. Nambu A, Takada M, Inase M, Tokuno H. Dual somatotopical representations in the primate subthalamic nucleus: evidence for ordered but reversed body-map transformations from the primary motor cortex and the supplementary motor area. J Neurosci 1996;16:2671–2683.
16. Rodriguez-Oroz MC, Rodriguez M, Guridi J, et al. The subthalamic nucleus in Parkinson's disease: somatotopic organization and physiological characteristics. Brain 2001;124(Part 9):1777–1790.
17. Romanelli P, Esposito V, Schaal DW, Heit G. Somatotopy in the basal ganglia: experimental and clinical evidence for segregated sensorimotor channels. Brain Res Brain Res Rev 2005;48:112–128.
18. Herzog J, Fietzek U, Hamel W, et al. Most effective stimulation site in subthalamic deep brain stimulation for Parkinson's disease. Mov Disord 2004;19:1050–1054.

19. Godinho F, Thobois S, Magnin M, et al. Subthalamic nucleus stimulation in Parkinson's disease: anatomical and electrophysiological localization of active contacts. J Neurol 2006;253:1347–1355.
20. Coenen VA, Prescher A, Schmidt T, Picozzi P, Gielen FL. What is dorso-lateral in the subthalamic Nucleus (STN)?—a topographic and anatomical consideration on the ambiguous description of today's primary target for deep brain stimulation (DBS) surgery. Acta Neurochir (Wien) 2008;150:1163–1165.
21. Maks CB, Butson CR, Walter BL, Vitek JL, McIntyre CC. Deep brain stimulation activation volumes and their association with neurophysiological mapping and therapeutic outcomes. J Neurol Neurosurg Psychiatry 2009;80:659–666.
22. Kuhn AA, Trottenberg T, Kivi A, Kupsch A, Schneider GH, Brown P. The relationship between local field potential and neuronal discharge in the subthalamic nucleus of patients with Parkinson's disease. Exp Neurol 2005;194:212–220.
23. Weinberger M, Mahant N, Hutchison WD, et al. Beta oscillatory activity in the subthalamic nucleus and its relation to dopaminergic response in Parkinson's disease. J Neurophysiol 2006;96:3248–3256.
24. Trottenberg T, Kupsch A, Schneider GH, Brown P, Kuhn AA. Frequency-dependent distribution of local field potential activity within the subthalamic nucleus in Parkinson's disease. Exp Neurol 2007;205:287–291.
25. Moran A, Bergman H, Israel Z, Bar-Gad I. Subthalamic nucleus functional organization revealed by parkinsonian neuronal oscillations and synchrony. Brain 2008;131(Part 12):3395–3409.
26. Marsden JF, Limousin-Dowsey P, Ashby P, Pollak P, Brown P. Subthalamic nucleus, sensorimotor cortex and muscle interrelationship in Parkinson's disease. Brain 2001;124:378–388.
27. Chen CC, Pogosyan A, Zrinzo LU, et al. Intra-operative recordings of local field potentials can help localize the subthalamic nucleus in Parkinson's disease surgery. Exp Neurol 2006;198:214–221.
28. Falkenberg JH, McNames J, Favre J, Burchiel KJ. Automatic analysis and visualization of microelectrode recording trajectories to the subthalamic nucleus: preliminary results. Stereotact Funct Neurosurg 2006;84:35–44.
29. Moran A, Bar-Gad I, Bergman H, Israel Z. Real-time refinement of subthalamic nucleus targeting using Bayesian decision-making on the root mean square measure. Mov Disord 2006;21:1425–1431.
30. Novak P, Daniluk S, Ellias SA, Nazzaro JM. Detection of the subthalamic nucleus in microelectrographic recordings in Parkinson disease using the high-frequency (>500 Hz) neuronal background: technical note. J Neurosurg 2007;106:175–179.
31. Rabiner LR. A tutorial on hidden markov models and selected applications in speech recognition. Proc IEEE 1989;77:257–286.
32. Zaidel A, Moran A, Marjan G, Bergman H, Israel Z. Prior pallidotomy reduces and modifies neuronal activity in the subthalamic nucleus of Parkinson's disease patients. Eur J Neurosci 2008;27:483–491.
33. Danish SF, Baltuch GH, Jaggi JL, Wong S. Determination of subthalamic nucleus location by quantitative analysis of despiked background neural activity from microelectrode recordings obtained during deep brain stimulation surgery. J Clin Neurophysiol 2008;25:98–103.
34. Deuschl G, Schade-Brittinger C, Krack P, et al. A randomized trial of deep-brain stimulation for Parkinson's disease. N Engl J Med 2006;355:896–908.
35. Saint-Cyr JA, Trepanier LL, Kumar R, Lozano AM, Lang AE. Neuropsychological consequences of chronic bilateral stimulation of the subthalamic nucleus in Parkinson's disease. Brain 2000;123 (Part 10):2091–2108.
36. Voon V, Kubu C, Krack P, Houeto JL, Troster AI. Deep brain stimulation: neuropsychological and neuropsychiatric issues. Mov Disord 2006;21:S305–S327.
37. Bejjani BP, Damier P, Arnulf I, et al. Transient acute depression induced by high-frequency deep-brain stimulation. N Engl J Med 1999;340:1476–1480.
38. Herzog J, Reiff J, Krack P, et al. Manic episode with psychotic symptoms induced by subthalamic nucleus stimulation in a patient with Parkinson's disease. Mov Disord 2003;18:1382–1384.